# Supporting Information

## Celik et al. 10.1073/pnas.0909456107

### SI Text

**Raman Spectroscopy.** ***Experimental procedure.*** The temperature controlled cell was observed with a WiTec Raman/near-field scanning optical microscope (WiTec Instruments Corp.) with an illumination line of 532 nm. A Nikon Air 50× (NA 0.55, long working distance) objective was used to collect Raman spectra of the ice and solution phases. The laser intensity was adjusted to 5 mW. The 5 µl sample was sandwiched between two cover glasses and placed on a temperature controlled metal plate. The sample was frozen by cooling the stage to −18 °C, then melted back to form individual ice crystals. The sample was heated slowly at a rate of not more than 0.01 °C/s, and the temperature was held constant at each stage of data collection. Raman spectra of ice below the melting point and ice in the superheated state were collected. Raman images were obtained by scanning an area and summing over it the ice OH stretching peak of the spectrum; see details in ref. 1. It took 4 min to collect a Raman intensity map of an area of 30 µm × 30 µm. For a full Raman spectrum from a single point, acquisition time was set to 1 min. In addition, bright light microscopy connected to a video camera was used and images were captured with a frame rate of 25 frames/s, which enabled us to measure melting velocities of superheated ice crystals.

**Results.** The series of images in Fig. S3*A* show an ice crystal formed in 72 µM *Marinomonas primoryensis* antifreeze protein (*Mp*AFP) solution at different superheating temperatures. This crystal was incubated for 45 min at 0.05 °C below its $T_m$ after which the temperature was slowly increased and images and single spectra were taken at different temperatures. The series of images in Fig. S3*B* show the Raman intensity map of a 30 µm × 30 µm section of the ice crystal before and after it was superheated. The melting for this particular crystal occurred at superheating of 0.37 °C, and the melting velocity of the ice front at the actual melting temperature ($T_{ms}$) was 106 µm/s. Raman spectra of ice were collected from the center of the crystal at different temperatures to observe whether there were any spectral changes prior to it going through its phase transition (Fig. S4). The spectrum of the crystal, with a local maximum around 640 nm, was virtually unchanged upon superheating, clearly indicating that the crystal is indeed superheated and still has an ice Ih structure. The transition in the spectrum from the ice phase to the melt phase was confirmed with repeated experiments ($n > 10$). Furthermore, the spectrum obtained just after the crystal melted (Fig. S4, purple line) was indistinguishable from the spectrum of the supercooled solution close to the crystal (Fig. S4, black line). The Raman spectra of the ice observed in these experiments are consistent with those obtained by others for ice Ih; see details in ref. 2).

To conclude, Raman spectroscopy experiments of ice in a supercooled solution and ice in superheated state show no difference in the spectra. The Raman signature of ice remained constant over the temperature changes until it melted. The spectrum of water is clearly different from that of ice. Thus we show that the ice maintains its integrity at superheated temperatures.

1.. Richardson HH, et al. (2006) Thermooptical properties of gold nanoparticles embedded in ice: Characterization of heat generation and melting. *Nano Lett* 6(4):783–788.

2.. Andreeva NP, Bunkin AF, Pershin SM (2002) Deformation of the Raman scattering spectrum of Ih ice under local laser heating near 0°C. *Opt Spectrosc (Transl of Opt Spektrosk)* 93(2):252–256.

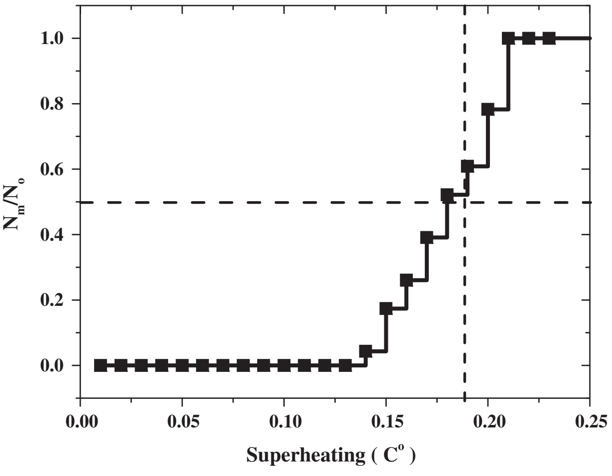


**Fig. S1.** Statistical analysis of melting as a function of superheating. A group of ice crystals ($N_0 = 23$) grown in *Mp*AFP solution are observed for their melting behavior at different superheating temperatures. The plot shows the ratio of the number of crystals that were melted ($N_m$) relative to the initial number of crystals ($N_0$) as a function of superheating ($T - T_m$). Half of the crystals melted when the sample was already 0.18 °C superheated.

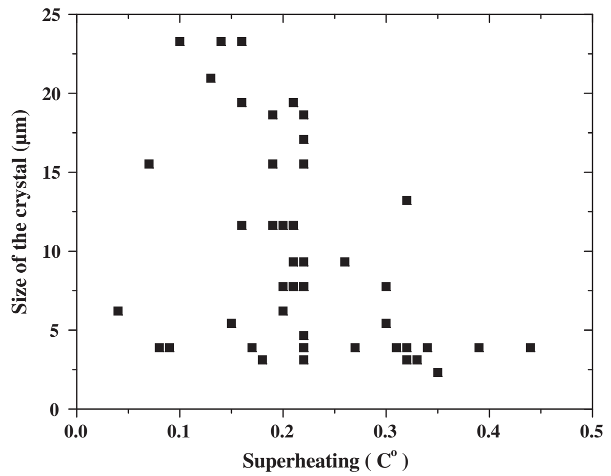


**Fig. S2.** Size distribution of the superheated ice crystals. A group of ice crystals ($N_0 = 51$) grown in *Mp*AFP solution were observed for their melting behavior over time as the temperature was increased slowly (see the main text for detailed information). Superheating values are shown as a function of the size of the ice crystals melted.

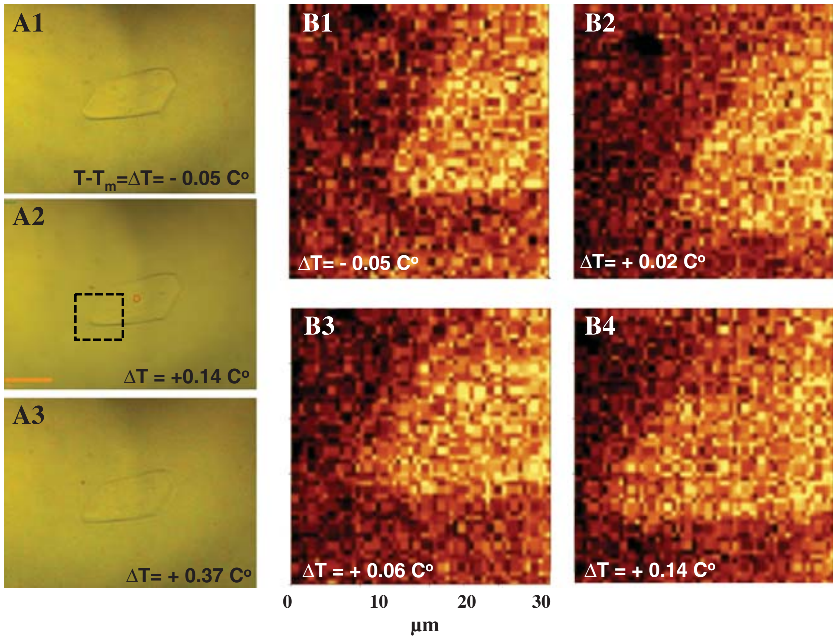


**Fig. S3.** Superheated ice crystal in *Mp*AFP solution. A single ice crystal at different temperatures is shown in images *A*1–*A*3. The scale bar shown in *A*2 is equivalent to 30 μm and applies to images *A*1–*A*3. The dashed rectangle indicates the area corresponding to the Raman intensity map of the 30 μm × 30 μm section of the ice crystal shown in images *B*1–*B*4. The pseudocolors in *B*1–*B*4 represent the intensity of the Raman spectrum around the ice peak (640 nm) at each point. Dark areas correspond to water, while bright areas represent ice. The red circular dot in the center of the crystal in *A*2 indicates where the laser was pointed to collect each individual Raman spectrum shown in Fig. S4.

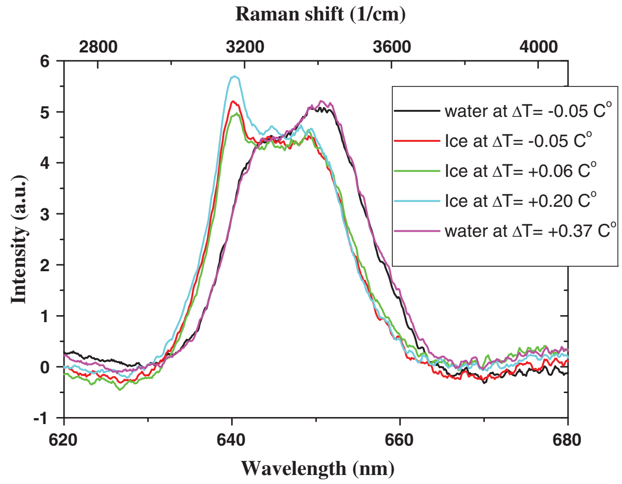


**Fig. S4.** Raman spectra of ice in *Mp*AFP solution. (*A*) The Raman spectra were obtained for solutions near the ice crystal, at the center of the ice crystal at different temperatures, and after ice melted at 0.37 °C above the melting temperature (purple line).

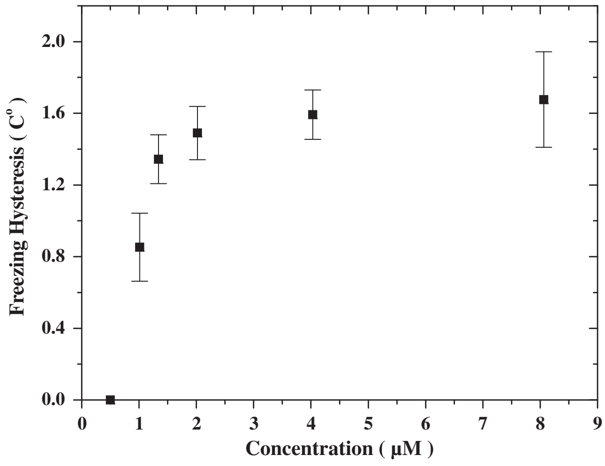


**Fig. S5.** Freezing hysteresis (FH) activity for GFP-*Mp*AFP: FH activity as a function of concentration is shown. These data were used in Fig. 4.

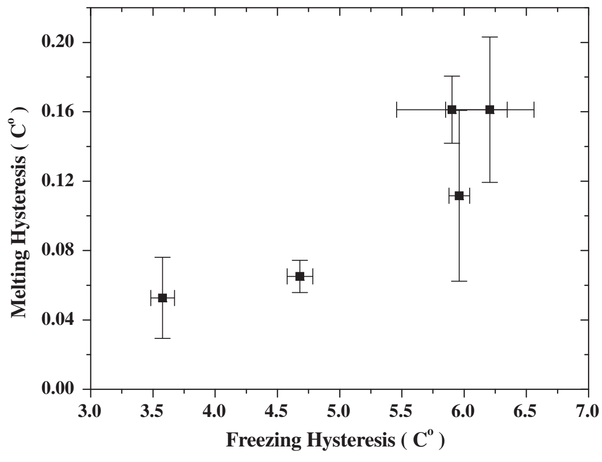


**Fig. S6.** Comparison of FH and melting hysteresis (MH) activity for *Dendroides canadensis* hemolymph. The measured MH values as a function of FH values at the corresponding concentrations are shown.

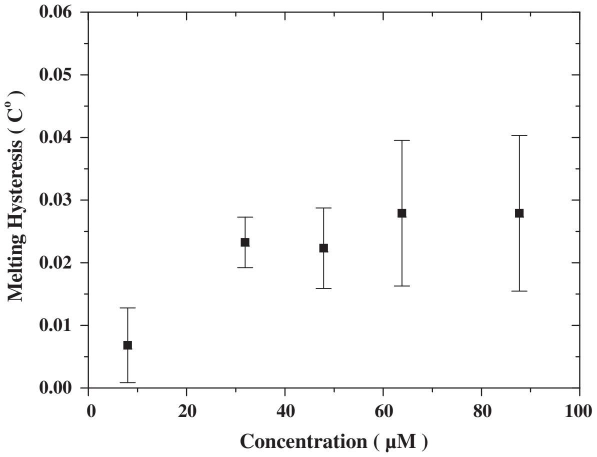


**Fig. S7.** Concentration dependence of MH activity for spruce budworm AFP (sbwAFP). MH activity for sbwAFP as a function of concentration.

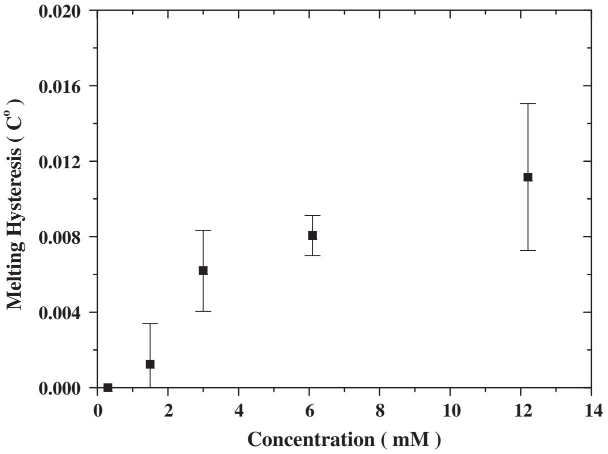


**Fig. S8.** Concentration dependence of MH activity for type I AFP. MH activity for type I AFP as a function of concentration.

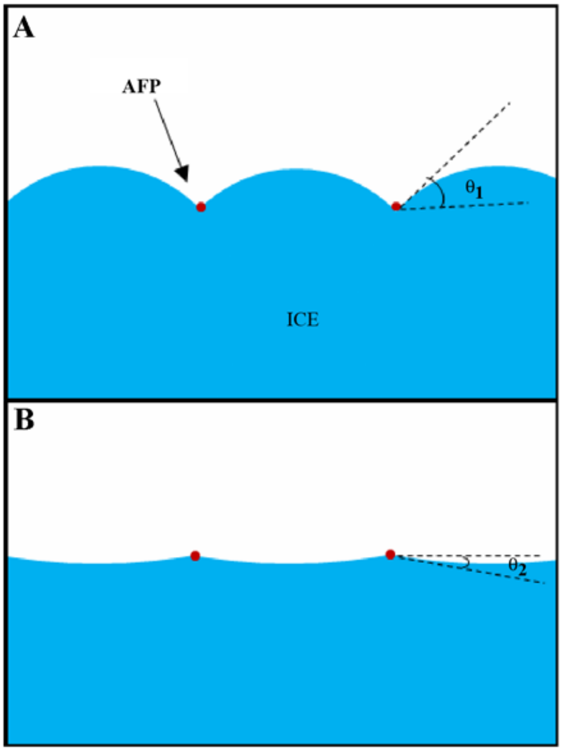


**Fig. S9.** Schematic model of the surface curvature of ice under supercooling and superheating conditions with adsorbed AFPs. (*A*) Under supercooling conditions, the ice develops a positive slope. (*B*) Under superheating conditions, a negative slope is formed. Dots represent adsorbed AFPs on the ice surface. The slopes are defined as $\chi_{\mathrm{engulfment}} = \tan(\theta_1)$ and $\chi_{\mathrm{superheating}} = \tan(\theta_2)$. An illustration of the time evolution of the surface curvature as a function of temperature is presented in Movie S1.

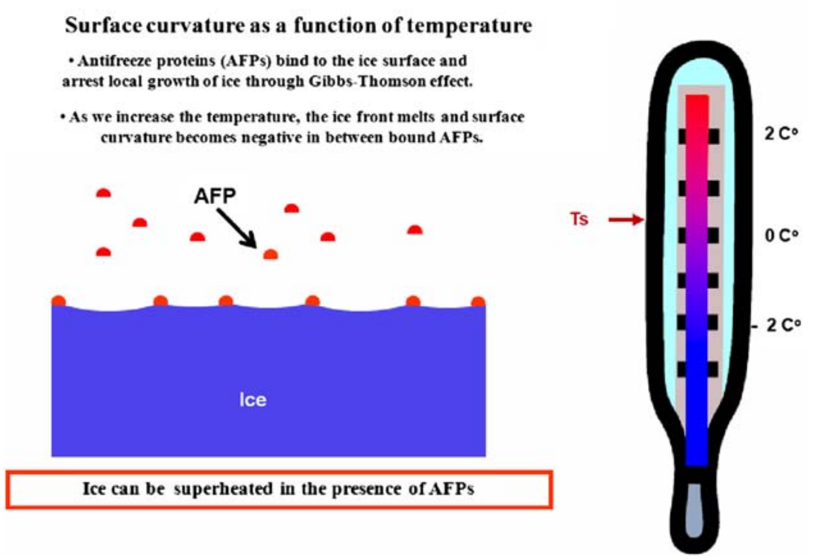


**Movie S1.** Illustration of surface curvature as a function of temperature. AFPs adsorb to the ice surface (red semicircles), causing ice growth or melting to occur along curved fronts in which the curvature increases as a function of supercooling or superheating. When the sample is supercooled, these ice fronts are concave, whereas they become convex when the sample is superheated.

Movie S1 (WMV)

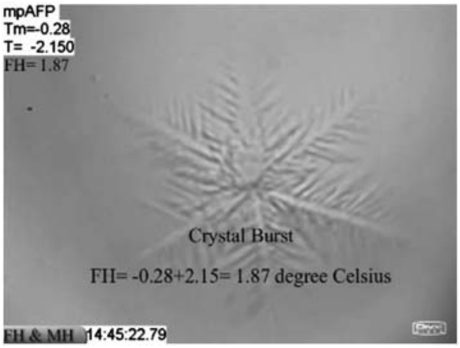


**Movie S2.** FH and MH experiment in a drop of *Mp*AFP solution. A movie of the experiment described in Fig. 1.
Movie S2 (WMV)


**Movie S3.** Melting experiment on a group of ice crystals. Ice crystals a solution containing the hyperactive AFP from *Tenebrio molitor* were examined in terms of their melting behavior in the same droplet while the temperature was slowly increased. The movie emphasizes the fast melting rates of the ice crystals above the $T_m (= -0.05\,°C)$. The last ice crystal melts at 0.18 °C above the $T_m$. The temperature of the sample is noted (*Upper Left*), and the real time during measurement is presented (*Lower Left*).
Movie S3 (WMV)